ILD CMP with Silica Abrasive Particles: Effect of Pore Size of CMP Pad on Removal Rate Profiles

Shoutian Li[z], Greg Gaudet, and Jayakrishnan Nair
Cabot Microelectronics Corporation, 870 N. Commons Dr. Aurora, IL 60504 USA

[z] E-mail: shoutian_li@cabotcmp.com

Abstract

The influence of pad intrinsic properties on the removal rate profiles of ILD CMP with fumed silica abrasive slurry was studied by changing pad's polymer hardness, porosity, and pore size. Of these intrinsic properties, pore size is found to be most critical to removal rate profiles. By systematically changing the pore size from <1μm to >100 μm, with porosity from 5% to 50%, of pad made of thermal-plastic urethane (TPU), removal rate profile of oxide polishing was studied. A flat removal rate profile cross wafer is desired for ILD CMP. It was found that when the pore size was larger than a certain threshold, flat removal rate profiles could be achieved. Below the threshold, severe edge-fast/center-slow removal rate profiles were observed and such profiles cannot be remedied by changing pad's other properties like porosity or polishing process conditions. A model is proposed to explain the non-flat removal rate profiles associated with the small pore size (<20 μm).

Introduction

The planarization of inter-level dielectrics (ILD) during the manufacturing ultra-large scale integrated (ULSI) devices has been achieved through chemical mechanical polishing (CMP) of silicon oxide layers using silica-based slurries.[1,2] The ILD CMP process has been widely studied.[3-6] Although the actual material removal in ILD CMP is a chemical process,[7] ILD CMP is widely considered as a mechanical process since the apparent material removal rate is proportional to mechanical input like polishing down force and rotational speeds.

The pad is an essential consumable besides slurry and conditioner that enable the ILD CMP process. A typical CMP pad for the ILD process is made of polyurethane in one of two forms: a thermal set urethane (TSU) or a thermal plastic urethane (TPU). Non-foamed polyurethane pad material has been used as ILD CMP pad[8] and has been found too difficult to be conditioned resulting in removal rate decay through the pad life.[9] Foamed polyurethane pads dominate the CMP pad market. The foaming methods include poromerics,[10-12] blending with microspheres,[13] frothing,[14] microcellular foaming,[15,16] blending with water-soluble polymeric spherical particles,[17-19] and embedding with mineral oil.[20] While the poromerics method provides open pore structures, all the other foaming methods mentioned above result in closed pores. Chemical blowing agents have been widely used in other industries but not in CMP pads because of the difficulty in quality control.[21] Giving the pad material, the foaming method and process controls the pad's intrinsic properties such as porosity and micro-porous structure (shape and size of the pores).

The impact of intrinsic pad properties on CMP material removal rate is a subject of many studies. Thakurta et al studied the pad porosity and compressibility in CMP.[22] Pad modulus is studied and modeled by many researchers.[6, 23-26] Bajaj et al found the oxide removal rate in ILD

polishing is proportional to pad porosity.[27] Pad surface roughness was studied by McGrath et al[28] and Park et al.[29] Lu et al studied the changes of pad pores on the surfaces.[30] Nevertheless, further understanding how pad properties affect CMP performance is needed.

In this paper, a systematical study of the effect of pore size in a pad with closed pores on the material removal rate was performed in ILD CMP with fumed silica slurry.

Experimental

CMP pad. – Pads with a systematical change in pore sizes were manufactured through CO_2 gas foaming of TPU with different polymer resin hardness.[16] By adjusting foaming conditions which can control pore size and porosity independently, the foamed sheets with pore sizes ranging from <1μm to over 100μm, and porosity ranging from 5% to 50% were obtained. The foamed sheet's porosity was determined by density measurement using ASTM standard D792. The porosity was calculated as:

$$\text{Porosity, \%} = (1 - \rho_{foam}/\rho_{solid}) \times 100 \qquad (1)$$

where ρ_{foam} is the foamed material's density and ρ_{solid} is the solid material's density. The pore size was reported as number average size measured from the cross-section SEM images (Model: AMRAY, KLA-Tencor, Corp., Milpitas, CA).

Unless specifically pointed out, all pads in this study were grooved as concentric grooving (20mil =508μm in groove width and 120mil = 3048μm in pitch, abbreviated as CC 20/120). The groove depth for the experimental pads were about 15mil (=381μm). However, the groove depth of commercial Epic™ D100 pad was 30mil (=762μm).

ILD CMP. – A commercial fumed-silica slurry Semi-Sperse™ 25 (SS25) (Cabot Microelectronics Corporation, Aurora, IL) was used in this study. The as-received slurry contained 25wt% solid at pH 11 and it was 1:1 diluted with laboratory-grade deionized water (DIW) (1 part of slurry and 1 part of water) at point-of-use (POU). ILD chemical mechanical polishing was conducted in a class I clean-room environment with a Mirra (200mm) polisher (Applied Materials, Santa Clara, CA). Unless specifically pointed out**,** the slurry flow rate was set at 200ml/min for Mirra. Wafers were 200mm 15K PETEOS (Advantiv Technologies, Inc. Fremont, CA). The change in monitor wafer thickness due to CMP was determined using a model KLA-Tencor UV-1050 (KLA-Tencor, Corp., Milpitas, CA). The removal rate was determined as the change in monitor wafer thickness per unit polishing time. The thickness of the wafers was measured cross the wafer diameter with 49 measurement points and 3 mm edge exclusion. Unless specifically pointed out**,** the conditioner was 3M A3700 diamond disk. 9lbf in-situ conditioning was applied in the experiments.

Pad surface textures characterization. - The pad surface micro-texture was characterized using a model μSurf® mobile LaserScope (NanoFocus AG, Oberhausen, Germany) and SEM (KLA-Tencor, Corp., Milpitas, CA). The LaserScope allowed on-platen data collection, e.g., measurement was done after certain number of polishing wafers and the pad was dried with compressed air without cutting or removal of the pad from polisher. Polishing was then resumed after the LaserScope measurement. The surface parameters like surface roughness etc were obtained using μSurf Analysis XT Verison 5.0.2 software.

Results

Impact of pad properties on material removal rate profile. – small pore size has been believed to be good for defectivity since the smaller volume of each pore is unlikely to trap larger, aggregate particles[9, 15,16, 20] and has potential to reduce slurry flow rate.[31] However, in this study, small pores (typically less than 20μm) are found to affect the profiles of material removal rate. A series of pads made of the same TPU polymer resin (72D in Shore D hardness scale) but with number average pore sizes of 2μm, 8μm, 27μm, 42μm and 70 μm were selected for Mirra polishing. Figure 1a shows the cross-section of SEM images of these pads and Figure 1b shows the pore size distributions. The commercial Epic™ D100 pad was included as baseline. The polishing down force was 4psi, the platen speed was 93rpm and the carrier speed was 87rpm. Figure 2 shows the profiles of the silicon oxide removal rates. For the pads with large pore sizes (27μm, 42μm and 70μm), the removal rates are flat cross the wafers if the rate drop off 1cm from edge is excluded. Such removal rate profiles are typical for industrial standard IC1010 and Epic® D100 pads. The rate drop off 1cm from edge is attributed to the rebounding effect when the retain ring of the carrier is pressed against the pad,[32] and it is beyond the scope of present study. On the other hand, the pads with small pore sizes (2μm and 8μm) show severely non-flat removal rate profiles – excluding the 1cm edge rate drop off, the removal rate gradually increases from wafer center toward to wafer edge. The removal rate difference between the 1cm from wafer edge and the wafer center can be > 2000Å/min.

Such big removal rate difference cross the same wafers was only found in pads with small pore sizes, regardless of porosity. Figure 3 shows the removal rate profiles from the three pads with the same small pore size (0.5μm) and made from the same polymer (72D) but 14%, 21% and 48% in porosity. ILD CMP was carried in Mirra polishing with 6psi polishing down force,

120rpm platen speed and 85rpm carrier speed. As seen from Figure 3, all three pads show the removal rates at wafer center much lower than near the wafer edge.

Changing polymer hardness does not change the shape of removal rate profiles as long as the pore sizes are small. Figure 4 shows the removal rate profiles from removal rate profiles of the experimental pads: (1) 42D polymer hardness, 55μm average pore size, 36% porosity, (2) 55D polymer hardness, 10μm average pore size, 30% porosity, (3) 75D polymer hardness, 6μm average pore size, 33% porosity and Epic™ D100 pad (72D polymer hardness, irregular pores of 5-100μm, 14% porosity). The data was obtained in Mirra polishing at 4psi, 93rpm of platen speed and 87rpm carrier speed. The 55D, 75D and D100 pads were grooved with concentric grooves (CC 20/120) but the 42D pad was grooved with XY (28mil =711μm in groove width and 250mil = 6350μm in pitch, abbreviated as XY 28/250). XY grooving is known to have lower ILD removal rate than concentric grooving. For example, the oxide removal rate of D100 pad with XY grooving is only half of the same pad with CC 20/120 grooving.[7] Both 55D (10μm) and 75D (6μm) pads have small pore sizes and both show severe non-flat removal rate profiles. On the other hand, the soft 42D with larger pore size (50um) shows normal flat removal rate profile as D100 pad. The data here, as well as other data that is not presented here, indicates the oxide removal rate profile is not flat by changing pad grooving from concentrate to XY as long as the pore size is below 20μm.

To better characterize the behavior of the non-flat removal rate profiles, we define center-slow wafer non-uniformity (CS-WNU, in %) as

$$\text{CS-WNU} = (RR_{max} - RR_{center})/RR_{center} \times 100 \quad (2)$$

where RR_{max} is the maximum of removal rate cross the wafer and RR_{center} is the removal rate at wafer center. CS-WNU is the indication how flat of the removal rate profiles cross the wafers. For an ideal flat profile, the CS-WNU is zero. Typically, the CS-WNU below 10% can be considered as acceptable for ILD CMP. The plot of CS-WNU as a function of pore size is shown in Figure 5. The data in Figure 5 was collected from the pads made of different TPU hardness and porosity. Clearly, to achieve flatter removal rate profiles, the pore size of a pad must be larger than a threshold about 20μm.

Besides ILD CMP, we also found the pads with small pore size (<20μm) caused non-flat removal rate profiles and unstable removal rate as a function of number of wafers polished in the other applications like Cu, barrier, and Al.

Attempts to flatten the removal rate profiles using CMP typical process knobs for the pads with pore size smaller than 20μm were not successful. These process knobs include adjusting zone pressure settings of Mirra or Reflexion polisher head (also known as "carrier"), polishing down force, slurry flow rate, slurry delivery location, different conditioning disks, and changing conditioner resident time etc. Simply reduce both platen and carrier speed at the same magnitude as described in the experimental section did not result in flat removal rate profiles as well.

However, a large offset of the carrier speed relative to platen speed can correct the removal rate profile. Such large offset in speeds is beneficial for the slurry flow underneath the wafer by avoiding back mixing,[33] as shown in Figure 6. The data in Figure 6 was obtained from a pad with 8 μm pore size, 24% porosity and 72D polymer hardness and concentric grooves (CC 20/120) at different polishing process settings. (a) is from the baseline process: polishing down

force (DF) was 4psi, the platen speed (PS) was 93rpm and the carrier speed (CS) was 87rpm, the retaining ring pressure (RRP) was 4.5psi and the inner tube (IP) pressure was 4psi. (b) was the same as the baseline except the RRP was increased to 7psi and the IP was increased to 6psi. (c) was the same as the baseline except the CS was reduced from 87rpm to 30rpm. Increase RRP and IP pressure made the profiles worse. Reduce the carrier speed relative to the platen speed dramatically can flat the removal rate profiles. It should be pointed out that the polisher manufacturer does not recommend any process with more than 15% difference in platen speed and carrier speed. Although the platen speed at 93rpm and the carrier speed at 30rpm can flatten the removal rate profile of the pad with 8 μm pore size, the > 300% difference in the platen and carrier speeds is not practical.

Although not practical, another way to flatten the TEOS removal rate profiles for the pad with small pore size (<20μm) was to condition excessively the pad area about 180mm wide covered by the 200-mm wafer track. Figure 7 shows the TEOS removal rate of a pad with 0.5 μm pore size, 48% porosity, 72D polymer hardness and concentric grooves (CC 10/80). The removal rate profile was not flat after 25 wafers polishing and became worse after 160 wafers polishing. However, additional pad break-in for 10 minutes with the disk sweeping from 40 mm to 220 mm relative to pad center, corresponding to the pad area about 180mm wide covered by the 200-mm wafer track, can flatten the removal rate profiles. This short range of pad conditioning can eventually result in un-even pad wear, thus, it is not practical solution to correct the un-even removal rate profiles.

Besides the unacceptable removal rate profiles, the pads with small pore size (<20μm) can also result in unexpected consequence on the wafer film. In a few experiments on a 300mm

Reflexion polisher, TEOS film de-lamination was observed from the pad with ~1μm pore size and ~15% effective porosity using silica-based SS25 ILD slurry. In the same experiments and under the same polishing conditions, the reference D100 pad did not de-laminate the TEOS wafers.

Surface micro-texture characterization of polished pads. – The surface micro-textures of the pads in above ILD CMP experiments were characterized by LaserScope and SEM. For the sake of clarity, the data of the pads with mean pore size 8μm (represent pads with small pore size) and 106μm (represent pads with large pore size) are presented here. Both pads were made of the polymer resin with 72D hardness (Shore D). The pad with mean pore size of 8μm has porosity of 23% and the pad with mean pore size of 106μm has porosity of 30%. ILD CMP with these pads was carried out on Mirra using SS25 slurry. The average of TEOS removal rates of these pads are similar (3720Å/min for the 8μm and 3650Å/min for the 100um) but CS-WNU are quite different: 48.3% for the 8μm vs 2.6% for the 106μm. The large CS-WNU indicates the large rate difference between the edge and the center of the wafers. To understand the performance difference, the pad surface micro-texture characterization was carried out with SEM and LaserScope. The scanning electron micrographs (SEMs) of the top surface of the polished pads are shown in Figure 8, in which (a) and (b) are from the 8μm pad and (c) and (d) are from the 106μm. The "furrows" seen from the SEMs are the results of diamond cutting from conditioning disks. The partial coverage of the pores seen in (c) and (d) is due to the plastic flow of the pad material. However, there is no observation that such pore partial coverage leads to removal rate or rate profile change.

LaserScope measurements show the surface of the 8μm pad is much smoother than the 106μm pad. The surface roughness, Sa, of the 8μm pad after polishing is 7.3μm (average of three different locations at 3, 5 and 8 inch from pad center) in contrast to 18.8μm of the 106μm pad. The surface probability density distribution of the two pads is shown in Figure 9. The pad with small pores shows lower asperities and shallow valley depth than the pad with large pores. The asperities are the contact sites for material removal to occur and the valley acts as slurry reservoir.

Discussion

ILD CMP with silica slurry is a mechanical-assisted chemical process in which actual removal is achieved by a direct nucleophillic attack of the silanolates of the silica particle on the wafer Si–O bond with the mechanical energy input via pad by providing the means to transport the slurry to the contact zone.[7] Because the slurry transport and mechanical energy in the contact zone are the keys to ILD removal, the removal rate shows strong dependence of mechanical characteristics. In moderate polishing down force (2 to 6psi) and speeds (60 to 110rpm), the silicon oxide removal rate is proportional to down force times speeds - a characteristics of Prestonian behavior, i.e., rate $\propto P \times V$.[34-42] Homma et al[43] reported that ILD removal rate was proportional to friction between wafer and pad during CMP. Recent work by Tamai et al[44] studied the relationship between mechanical energy and material removal rates of different abrasive particles. They found Si, SiO_2 and Si_3N_4 removal rates are proportional to mechanical energy in the contact zone. Since the polishing was carried out under the same CMP process setting for the different abrasive particles which could have different removal rates, this finding implies that the different abrasive particles can have different efficiency in converting the total mechanical energy input from the CMP processes for the use of material removal. On the other

hand as demonstrated in our previous publication, the different pad surface textures can also have different efficiency to convert the total mechanical energy input from CMP processes.[7]

The influence of a pad's properties on the removal rate is the subject of many studies. For example, pad's porosity on silicon oxide removal rate was studied by Bajaj et al.[27]. Pad's porosity and compressibility on CMP rate was studied by Thakurta et al.[22] . Pad's surface roughness was studied by Park et al.[29] and Park et al. [45] and modeled by Castillo-Mejia et al.[46] Pad's grooves provide macro-texture to transport slurry to the contact zone and the groove designs have been the subjects of many studies[7,47-49]. Pad's asperities were studied by Muldowney[50] and the influence of pad conditioning on SiO_2 removal rate was studied by Lawing.[51-53]

The present study focuses on the intrinsic properties of pad – particularly on pad pore size and its influence on the ILD removal rate profiles. The pad with small pore sizes has shown un-even removal rate profiles in which the rate near edge is significantly higher than the rate at wafer center. Such removal rate profiles are the characteristics associated with small pore sizes and are hard to be remedied through typical CMP process tuning. As demonstrated in Figure 3 and Figure 4, the responsibility to the un-even removal rate profiles by other pad intrinsic properties, namely, polymer hardness, pad porosity and pore morphology can be ruled out. The pads in this study have closed pores. As seen in Figure 1a, the reference D100 pad has irregular pore morphology and the other test pads have spherical pores. In addition, we also tested the commercially available pads with open pore structure like Fubjibo and Politex. The TEOS removal rate profiles of these two pads were like that of D100.

The small pore size results in two consequences. First, the small pore sizes reduce slurry holding capacity. The porosity in pad is created by closed pores. In a simple model, let's assume: (1) all pores have the same size with radius, r; (2) all pores are randomly and homogenously distributed in the polymer matrix; (3) only those pores that are open to surface can have opportunities to hold slurry. Thus, the slurry holding capacity per unit surface area, C, is equal to

$$C = r \times P \qquad (3)$$

where P is the porosity, r is the radius of a pore. Table 1 shows the slurry holding capacity comparison among the pads with different pore size and porosity. The slurry holding capacity per unit surface area by concentric grooves with 20mil groove width, 120mil pitch and 15mil groove depth (CC20/120/15) is included for comparison. Although a groove's slurry holding capacity is more than the capacity of the surface pores, it is the slurry on the land area that actually contributes to material removal. It can be seen from Table 1, for the pad with large pores (100μm) and high porosity (45%), the slurry holding capacity by pores per unit surface area can reach one third of the holding capacity of concentric grooves (CC20/120/15). At constant porosity, reduce pore size will reduce slurry holding capacity. For example, change pore size from 50μm to 5μm will result in 1 order magnitude reduction in slurry holding capacity. Low slurry holding capacity means there are less slurry particles available for the asperities to transport them into contact zone, implying low removal rate. However, this slurry holding capacity alone cannot explain the removal rate profiles of the pads with small pores. If lower slurry holding capacity means less abrasive particles to have enough kinetic energy (i.e., mechanical energy) for the direct nucleophillic attack on the wafer Si–O bond, overall lower removal rate is expected but not un-even removal rate profile.

Second, the small pore sizes results in smoother pad surface with low height of asperities as seen from Figure 8 and Figure 9. Pad relies on conditioning to rejuvenate pad asperities, as documented in early ILD CMP studies.[54-56] However, using a 4-inch conditioner to a 20-inch or 30-inch pad is not an efficient process. Depending on the diamond conditioner type, the sizes of diamonds are in the range of a hundred to several hundred micrometers and the shapes can be classified as sharp or bulky. Typically small and sharp diamonds can provide better cutting to CMP pad and better efficiency to restore pad asperities than large and bulky diamonds. As the pad pore size becomes smaller, especially below 10μm, it is more difficult for the diamonds, which are more than 10 times larger the pores now, to grab the edge of pores for efficient cutting. Eventually glazing of pad surface dominates rejuvenation of pad asperities by diamond conditioning, results in declining polishing rate with pad life. This is similar to the solid pad (non-foamed pad) situation. The solid ILD pad was found too difficult to be conditioned and the oxide removal rate decayed through the pad life.[8,9]

The smooth surface will increase the adhesion force between the wafer and pad surface with the presence of slurry. This in turn may lead to higher adhesion friction. According to the work by Homma et al.[43], high friction will lead to higher removal rate. Thus, we can postulate the friction force at the edges of the wafers for the pads of 2μm and 8μm in Figure 2 will be more than 25% greater than the friction force for the pads with large pores (27μm, 42μm and 70μm) since at near wafer edge, the pads with small pore size show higher removal rates compared to pads with large pores. However, the removal rate is proportional to friction understanding is only valid when there is enough slurry between wafer and pad in boundary lubrication regime. If there is no slurry or very little slurry, the contact between wafer and pad

becomes “dry” contact. Such dry contract can lead to very high friction but does not contribute to material removal on wafer.

The mechanistic picture emerges for the removal rate profiles associated with the pads with small pores. The small pores of the pads result in high adhesion friction, which can lead to high removal rate near the wafer edge. However, the high adhesion also prevents the fresh slurry flow into wafer center, resulting slurry “starvation”. Thus, the “dried” pad underneath the wafer can have very high friction. This explains the TEOS-film de-lamination phenomenon observed in some of our 300mm wafer ILD tests with small pore pads. On the other hand, at the edge of wafer the suction force created by the motion of wafer and pad can still pull slurry in. Thus, the combination of high adhesion friction force at the edge of the wafer and slurry starvation at center of the wafer results in the large difference in material removal rate cross the wafer, i.e., edge fast but center slow removal rate profiles. A fluid dynamic simulation is under way in our laboratory to further understand this phenomenon.

Conclusion

The removal rate profiles of ILD CMP using fumed silica slurry were systematically studied as a function of pad’s pore size ranging from <1 μm to >100 μm. For the pad’s pore size below 20 μm, TEOS removal rate profiles are un-even. Such un-even removal rate profiles are the characteristics of small pore pores regardless of pad’s other intrinsic properties like polymer hardness, porosity and pore morphology. It is difficult to find practical CMP process knobs to flatten the removal rate profiles. On the other hand, the problem can be corrected by increasing pad pore size greater than 20μm. The un-even removal rate profiles associated with small pores of the CMP pads can be attributed to the strong adhesion friction force created by the small pores

on the pad surface, which enhances material removal rate at wafer edge and the same time decreases rate at wafer center through the reduction of slurry flow.

Acknowledgement

The authors would like to thank Dr. Fred Sun, Dr. Michael Lacy and Dr. David Boldridge for their constructive comments and suggestions. The authors thank Cabot Microelectronics Corporation for permission to publish this work.

Figure captions:

Figure 1a. The cross-section of SEM images of the pads with number average pore sizes of 2μm (a1), 8μm (a2), 27μm (a3), 42μm (a4), 70 μm (a5) and D100 (a6).

Figure 1b. The pore size distribution plot of the pads with number average pore sizes of 2μm, 8μm, 27μm, 42μm and 70 μm.

Figure 2. The removal rate profiles of the pads with number average pore sizes of 2μm, 8μm, 27μm, 42μm and 70 μm.

Figure 3. The removal rate profiles of the pads with the same small pore size (0.5μm) but 14%, 21% and 48% in porosity.

Figure 4. The removal rate profiles of the 42D (55μm), 55D (10μm), 75D (6μm) and D100 pads.

Figure 5. The plot of CS-WNU as a function of pore size.

Figure 6. The TEOS removal rate profiles of the pad with 8μm pore size at the at different polishing process settings. (a) the baseline process: DF= 4psi, PS= 93rpm, CS = 87rpm, RRP = 4.5psi and IP = 4psi. (b) The increased RRP/IP: same as the baseline except the RRP = 7psi and the IP = 6psi. (c) The reduced carrier speed: same as the baseline, except the CS = 30rpm.

Figure 7. The TEOS removal rate profiles of the pad with 0.5μm pore size. (a) after 25 wafers polishing. (b) after 160 wafers polishing. (c) additional 10-minute pad break-in at the pad area covered by the wafer track.

Figure 8. The scanning electron micrographs (SEMs) of the top surface of the polished 8μm and 106 μm pads. (a) 8μm at 107x and (b) 8μm at 500x; (c) 106μm at 110x and (b) 106μm at 500x.

Figure 9. The surface probability density distribution of the top surface of the polished 8μm and 106 μm pads.

Fig.1a

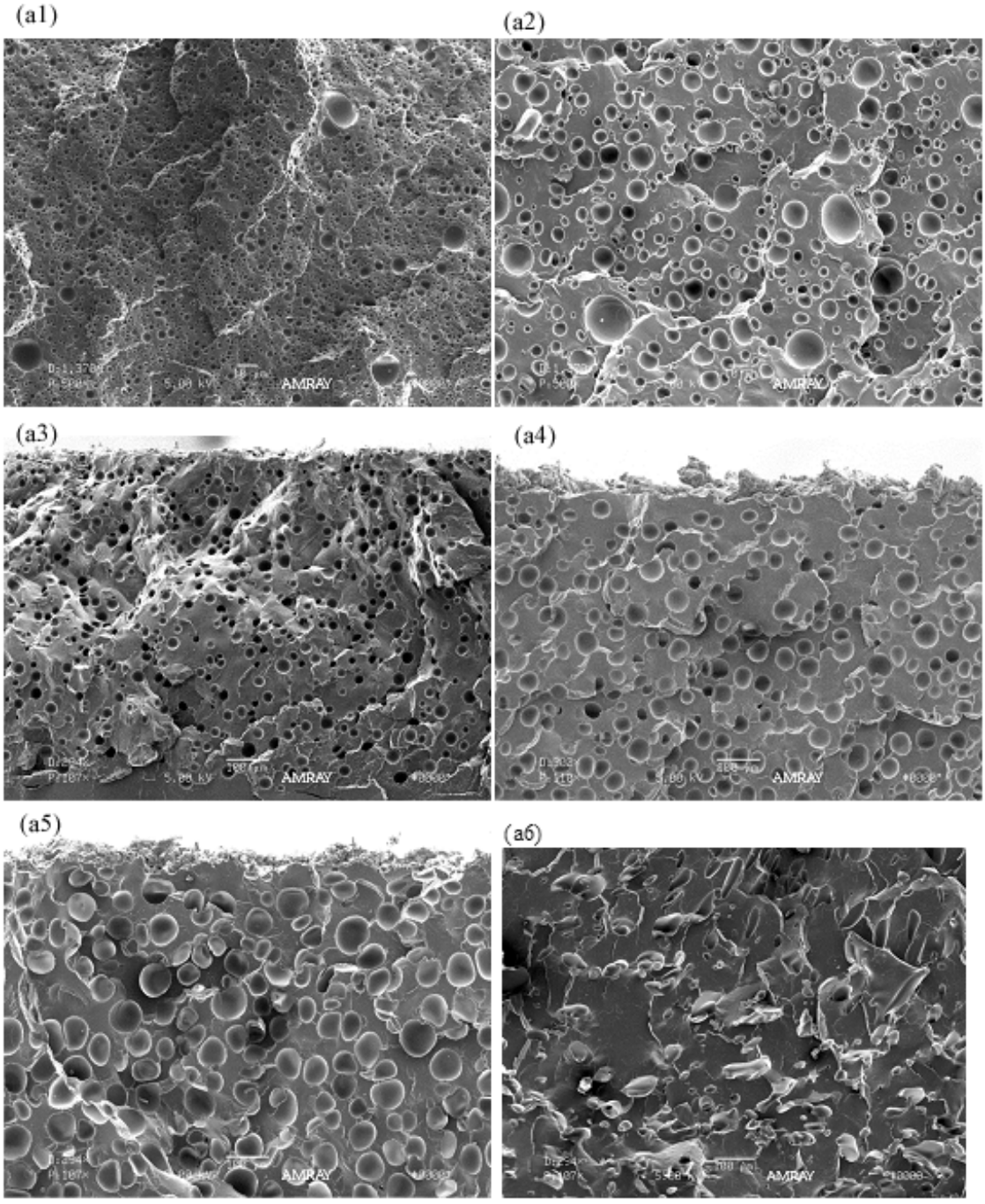

Fig.1b

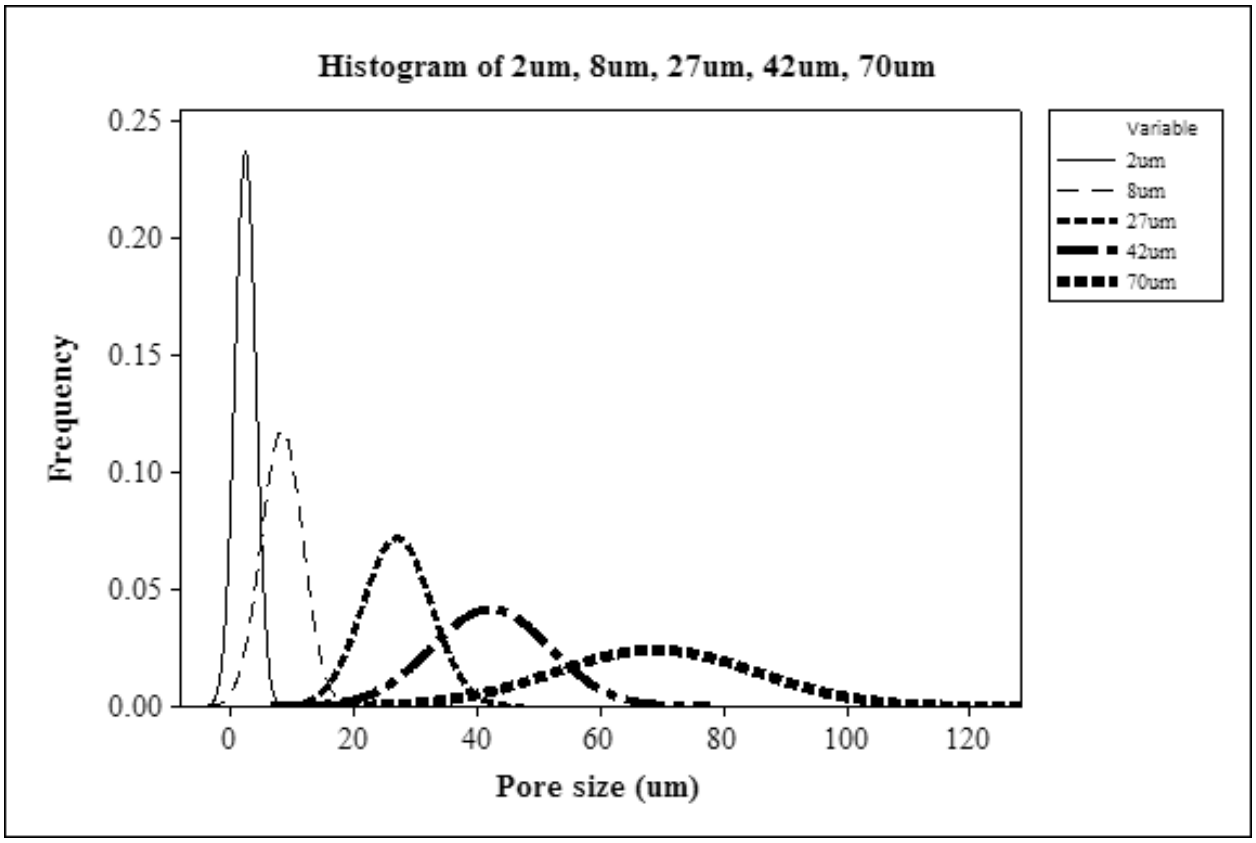

Fig.2

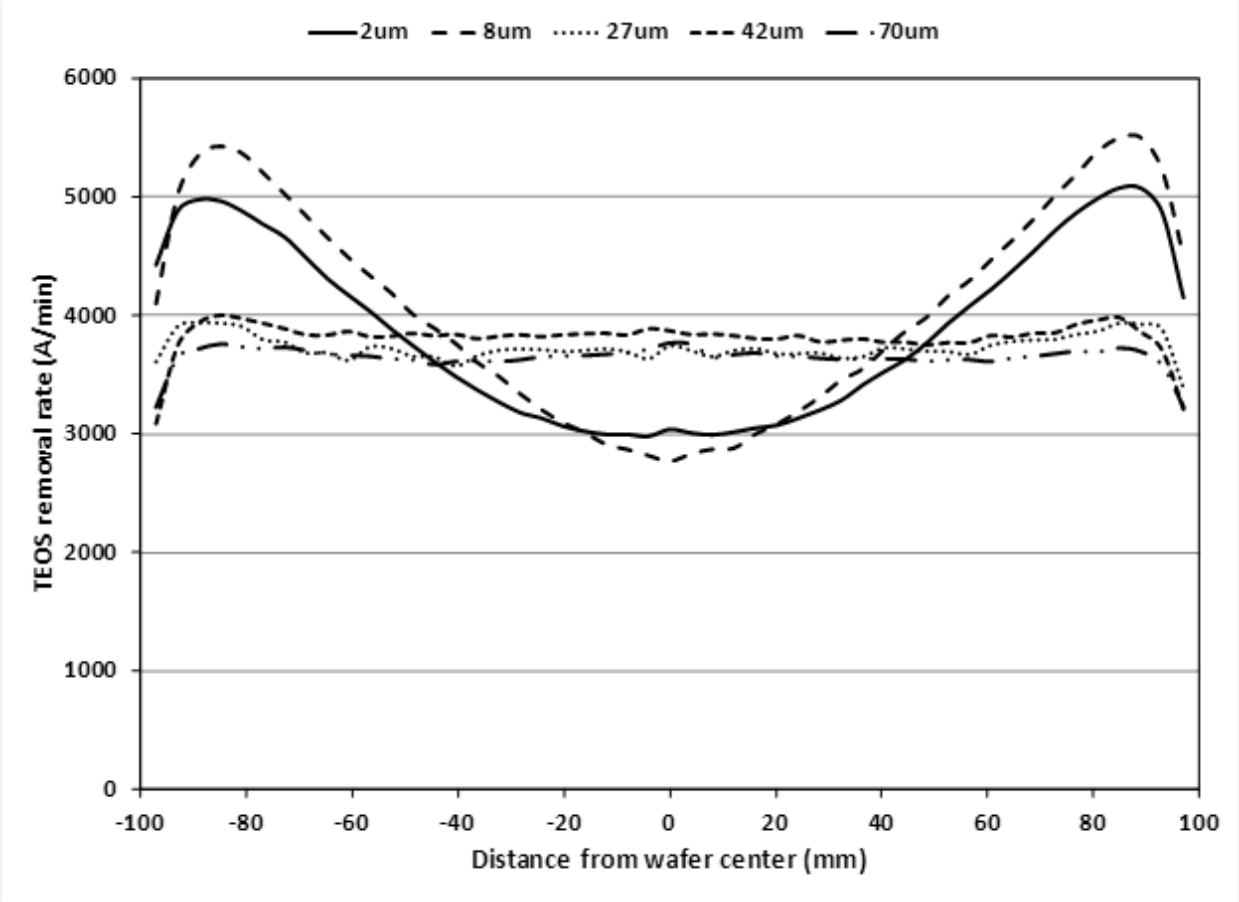

Fig.3

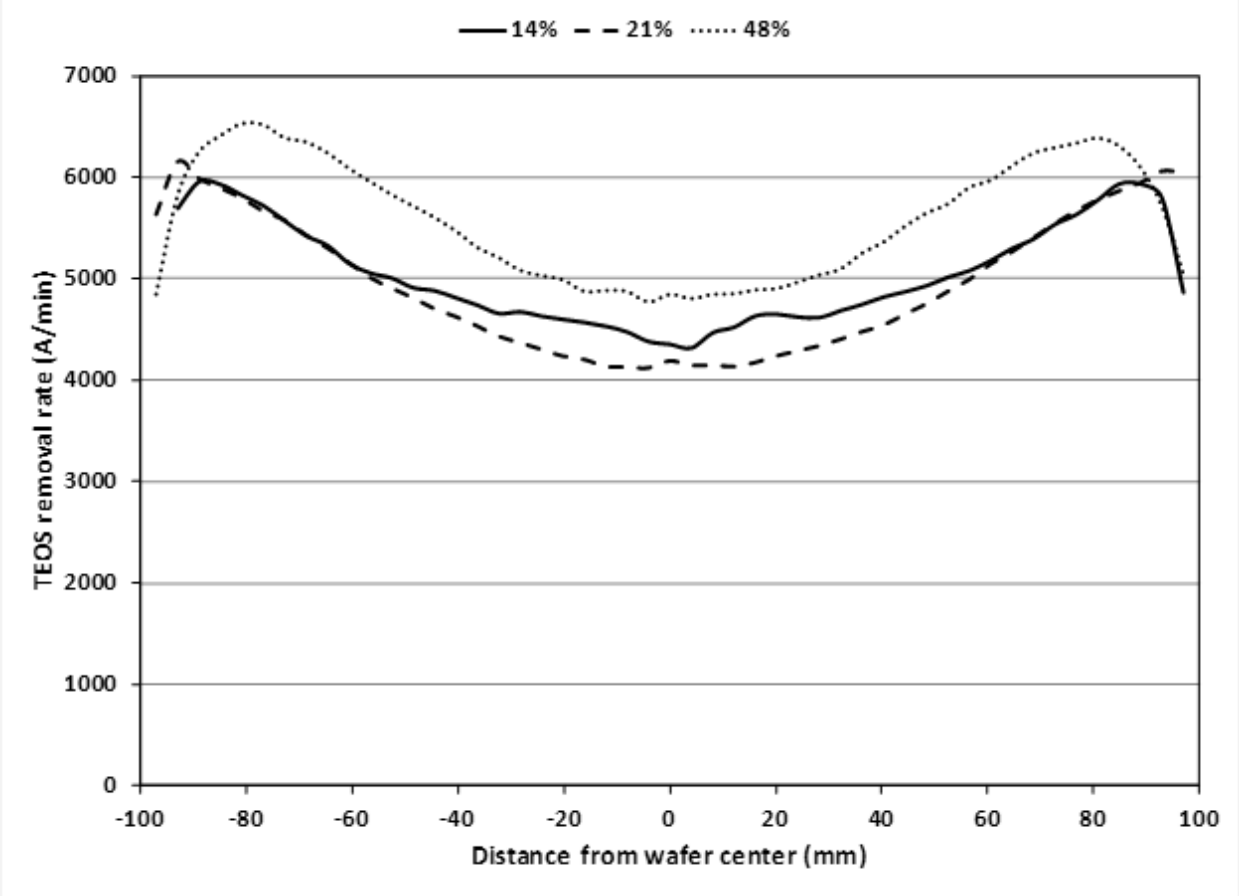

Fig.4

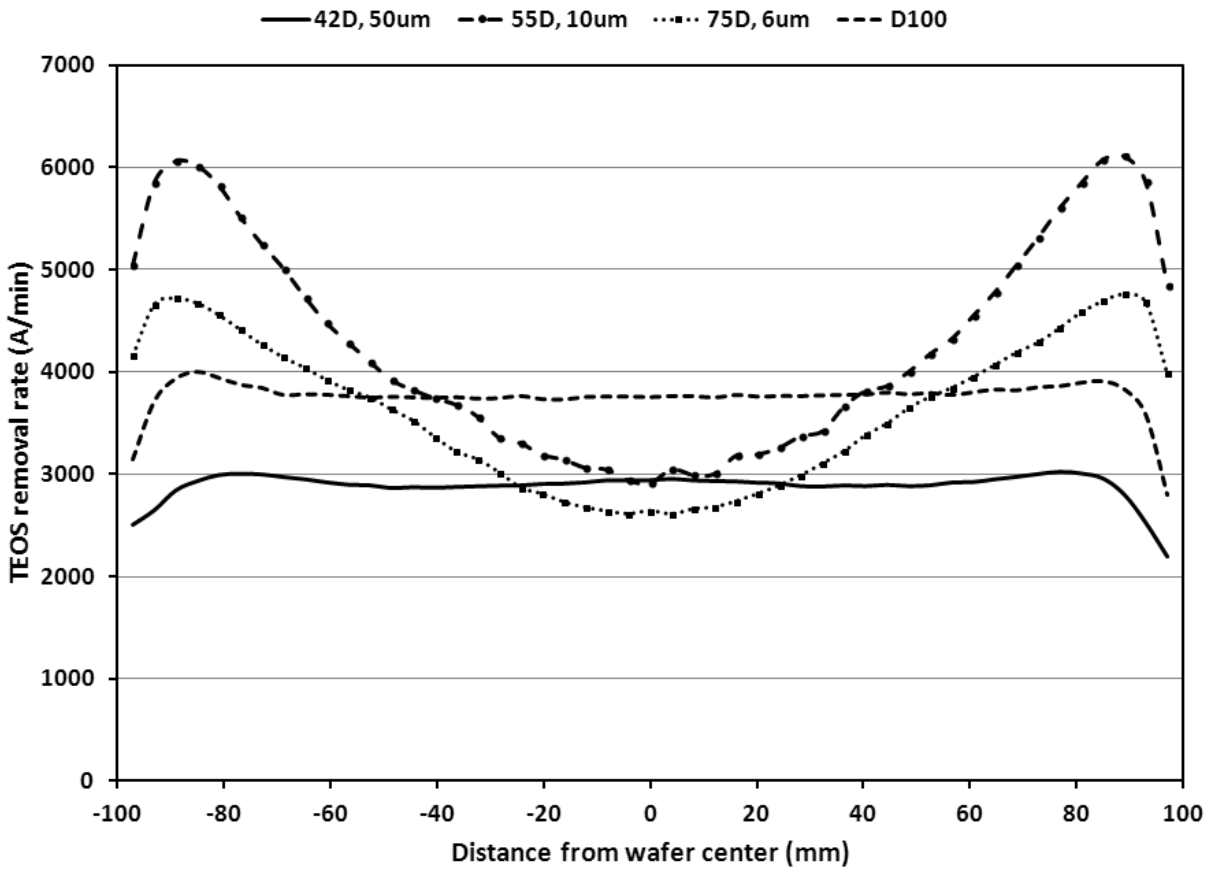

Fig.5

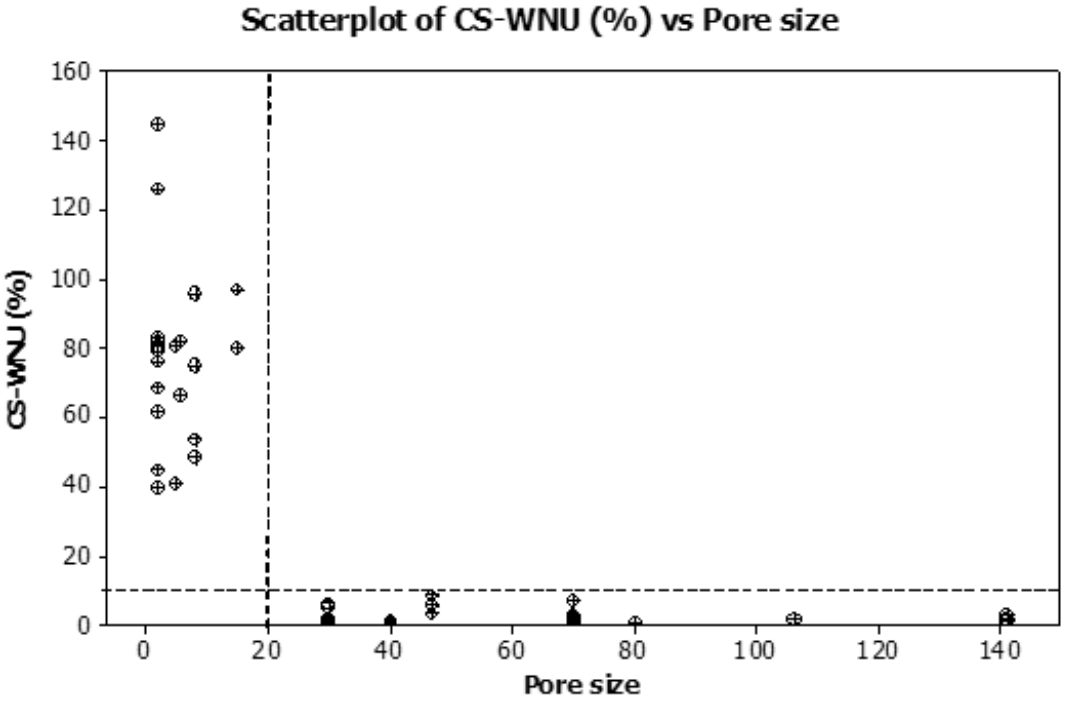

Fig.6

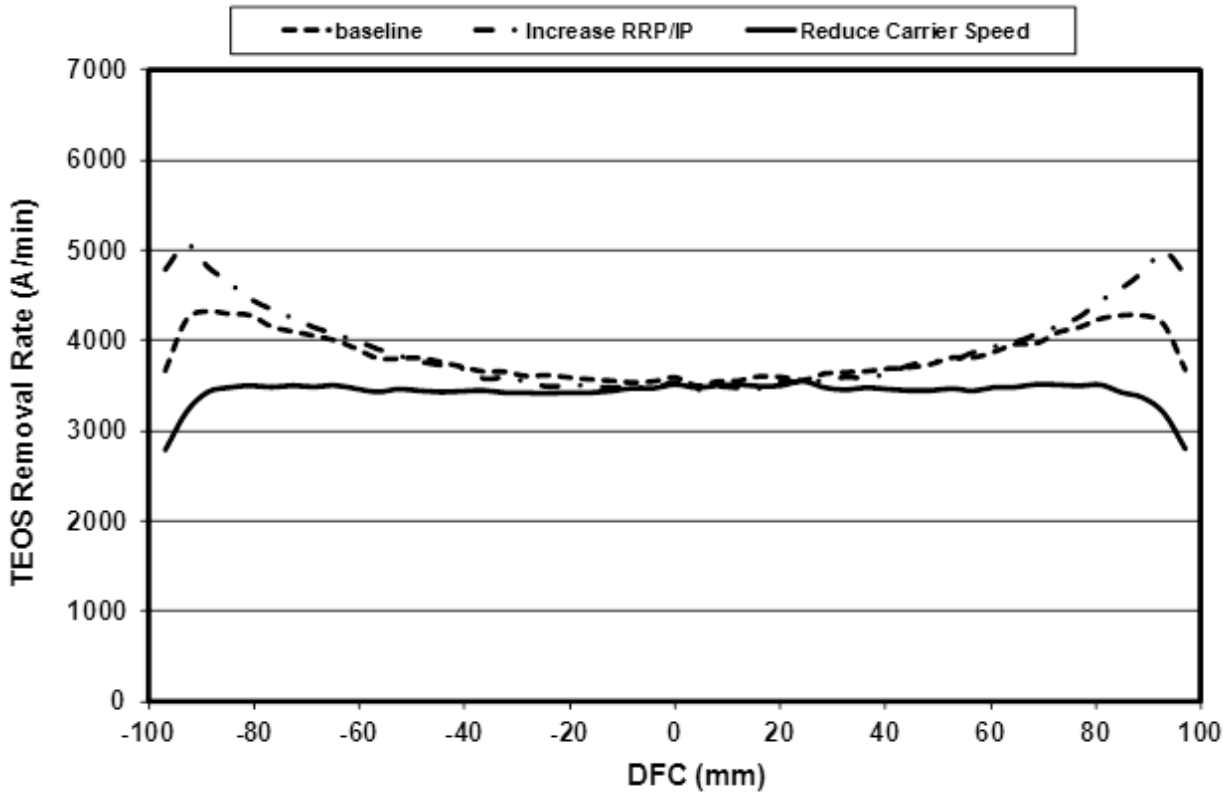

Fig.7

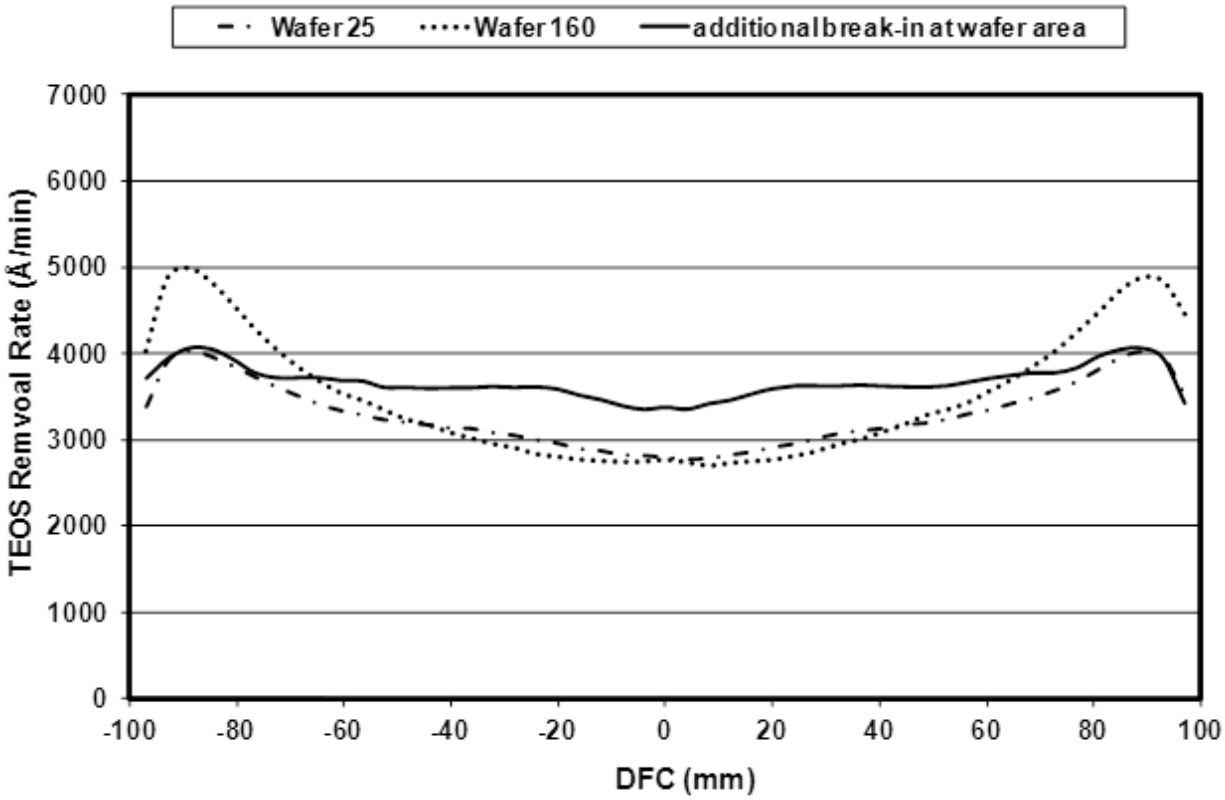

Fig.8

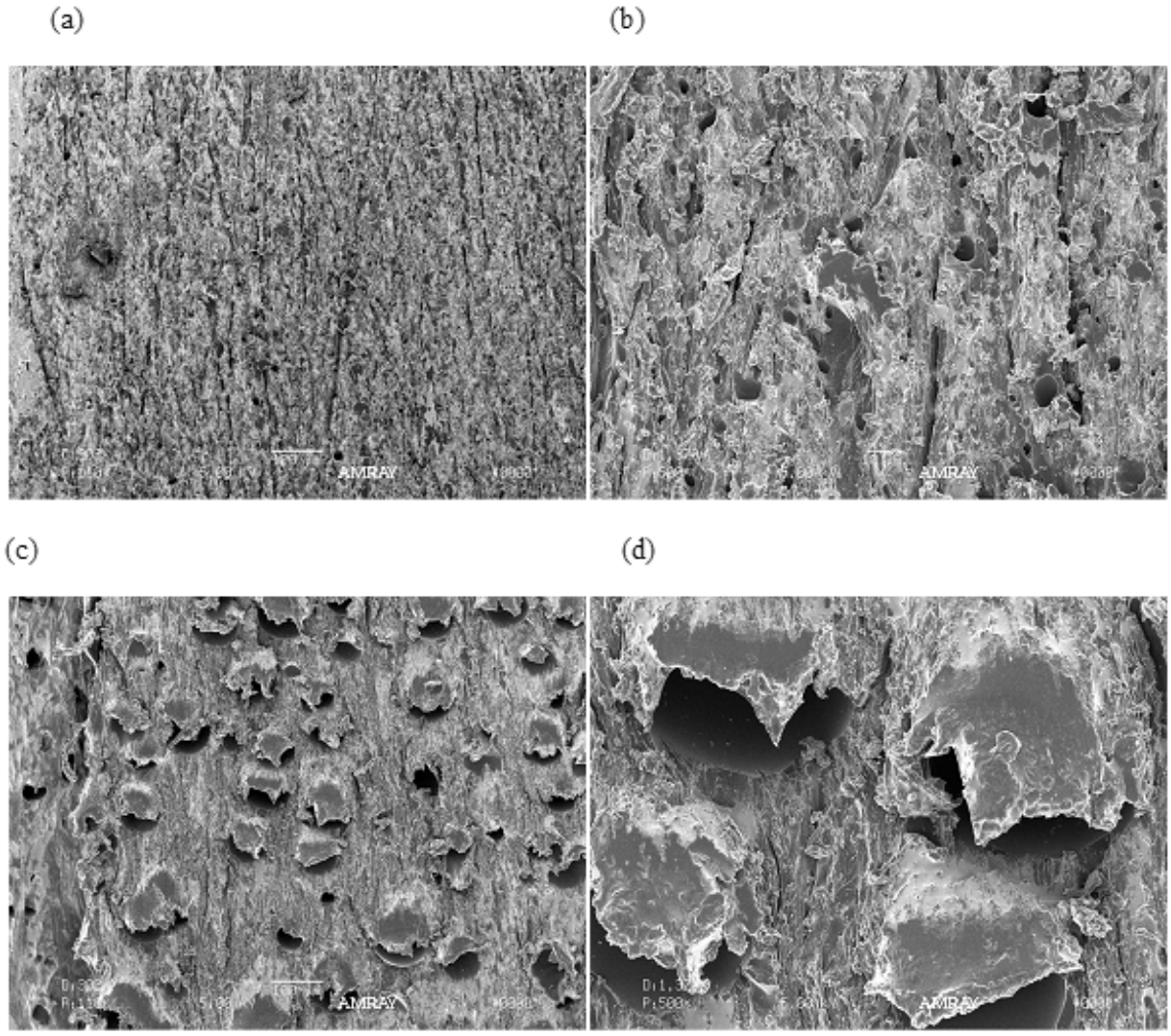

Fig.9

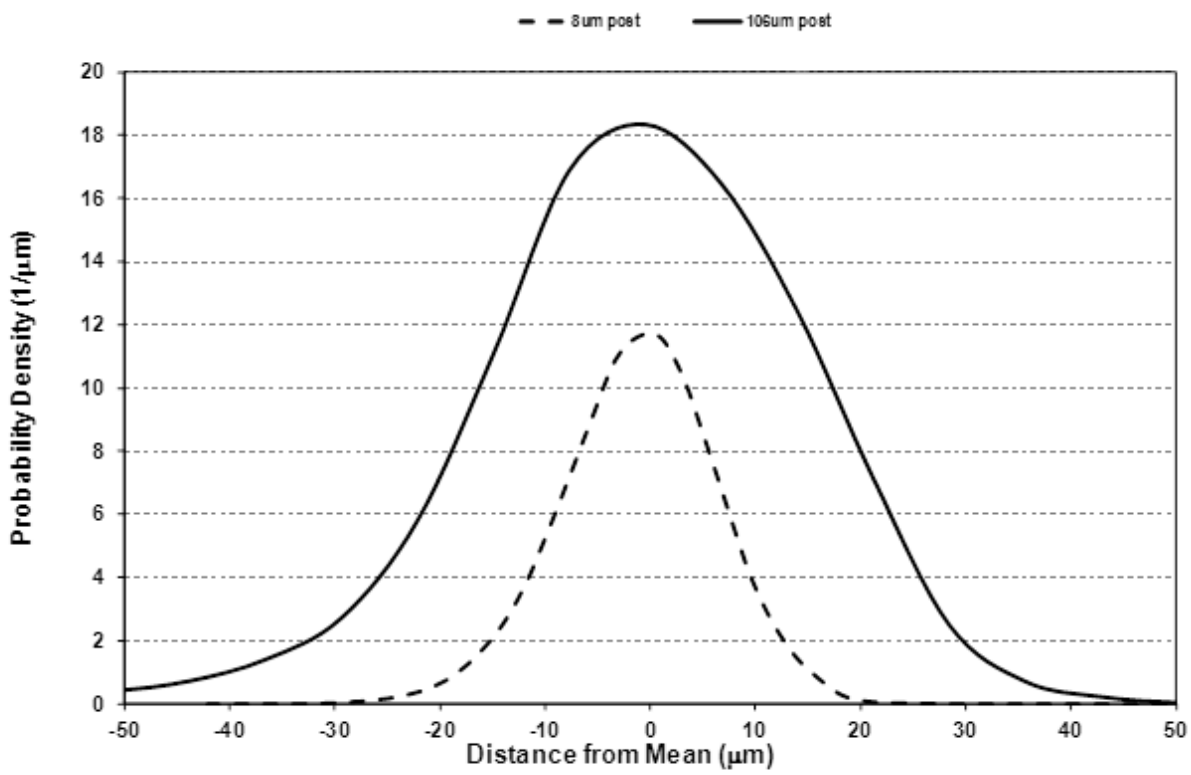

Table 1. The calculation of slurry holding capacity per unit surface area at different pore size and porosity. The slurry holding capacity by grooves is included for comparison.

Example	Pore size (μm)	Porosity (%)	Slurry holding capacity ($\mu m^3/\mu m^2$)
1	0.5	15	0.0375
2	5	15	0.375
3	50	15	3.75
4	100	45	22.2
5	Concentric grooves (20mil groove width, 120mil pitch and 15mil groove depth)		76.29

Reference

1. J. Steigerwald, S. Murarka and R. Gutmann, *CMP of Microelectronic Materials*. , Wiley, New York (1996), P129-304.
2. M. F. Chow, W. L. Guthrie, and F. B. Kaufman, US Patent 4,702,792 (1987).
3. K. Achuthan, J. Curry, M. Lacy, D. Campbell, and S. V. Babu, *J. Electronic Mater*., **25**, 1628 (1996).
4. A. K. Sikder, F. Giglio, J. Wood, A. Kumar, and M. Anthony, *J. Electronic Mater*., **30**, 1520 (1996).
5. L.J. Borucki, T. Witelski, C. Please, P. R. Kramer, and D. Schwendeman, *J. Engineering Mathematics*. **50**, 1 (2004).
6. S. Oh, and J. Seok, *Wear*, **266**, 839 (2009).
7. S. Li, G. Gaudet, F. Sun and A. Naman, *J. Electrochem. Soc*. **157(11)**, H1061 (2010).
8. L. M. Cook, J. V. H. Roberts, C. W. Jenkins and R. R. Pillai, US Patent, 5,489,233 A (1996).
9. D. B. James, in *Chemical-mechanical planarization of semiconductor Materials*, Ed. By M. R. Oliver, Springer, pp167-213 (2004).
10. D. G. Hulslander and W. F. Manwaring, US Patent, 3,284,274.
11. M. F. Hoffstein and T. Shinagawa, European Patent, EP0304645 B1.
12. T. Twase and T. Iwao, US Patent, 7,897,250 B2.
13. H. F. Reinhardt, J. V. H. Roberts, H. G. McClain, W. D. Budinger and E. W. Jensen, US Patent, 5,578, 362; US Patent, 5,900,164; US Patent, 6,439,989 B1
14. R. D. Duffy, US Patent, 5,604,267
15. A. Prasad, US Patent, 6,913,517 B2.
16. A. Prasad, US Patent, 7,267,607 B2.
17. H. Shiho, H. Aoi, and K. Hasegawa, European Patent, 1,418,921 B1.
18. H. Shiho, H. Aoi, K. Hasegawa and N. Kawahashi, US Patent, 6,992,123 B2.
19. H. Shiho, K. Hasegawa and N. Kawahashi, US Patent, 7,183,213 B2
20. H. Huh, S. M. Lee, K. C. Song, S. G. Kim, and D. K. Son, US Patent, 7,579, 071B2
21. B. Lombardo, US Patent, 6,514,301 B1
22. D. G. Thakurta, C. L. Borst, D. W. Schwendeman, R. J. Gutmann, and W. N. Gill, *Thin Solid Films*, **366**, 181 (2000).

23. L. Lu, Y. Obeng, and K. A. Richardson, *Materials Characterization*, **49**, 177 (2002).
24. J. J. Vlassak, *J. Mechanics and Physics of Solids*, **52**, 847 (2004).
25. W. Li, D. W. Shin, M. Tomorzawa, and S. P. Murarka, *Thin Solid Films* **270**, 601 (1995).
26. K. Qin, B. Moudgil, C. W. Park, *Thin Solid Films* **446**, 277 (2004).
27. R. Bajaj, M. Desai, R. Jairath, M. Stell, and R. Tolles, *Mat. Res. Soc. Symp. Proc*. **337**, 637 (1994).
28. J. McGrath and C. Davis, *J. Materials Processing Technology*, **153-154**, 666 (2004).
29. K. H. Park, H. J. Kim, O. M. Chang, and H. D. Jeong, *J. Materials Processing Technology*, **187-188**, 73-76 (2007).
30. H. Lu, B. Fookes, Y. Obeng, S. Machinski, K. A. Richardson, *Materials Characterization*, **49**, 35 (2002).
31. P. K. Roy, M. Deopura and S. Misra, US Patent, 7,704,125 B2
32. R. Bajaj, S. Hymes, N. Vaduri, and S. Fisher, *22nd CMPUG*, Ludwigshafen, Germany (2009).
33. G. P. Muldowney, *Mat. Res. Soc. Symp. Proc*. **Vol 816**, K5.3.1 (2004).
34. F. Preston, J. Soc. Glass Technol. 11, 247 (1927).
35. W. T. Tseng, and Y. L. Wang, *J. Electrochem. Soc*. **144**, L15 (1997).
36. Maury, D. Ouma, D. Boning and J. Chung, *Advanced Metalization and Interconnect Systems for ULSI Applications*, Sept. 30- Oct. 2, (1997).
37. P. Wrschka, J. Hernandez, Y. Hsu, T. S. Kuan, G. S. Oehrlein, H. J. Sun, D. A. Hansen, J. King and M. A. Fury, *J. Electrochem. Soc*. **146**, 2689 (1999).
38. F. Zhang and A. Busnaina, *Electrochemical and Solid-State Letters*, **1**,184 (1998).
39. B. Zhao and F. G. Shi, *1999 CMP-MIC conference*, pp. 13-22, Santa Clara, CA, Feb. 11-12, (1999).
40. Q. Luo, S. Ramarajan, and S. V. Babu, *Thin Solid Films*, **335**, 160 (1998).
41. J. Luo, "Review of Chemical-Mechanical Planarization Modeling for Integrated Circuit Fabrication: From Particle Scale to Die and Wafer Scales", *2002-2003 LMA Reports*, University of California at Berkeley, pp. 107-135.
42. L. Guo and R. S. Subramanian, *J. Electrochem. Soc*. **151**, G104 (2004).
43. Y. Homma, *J. Electrochem. Soc*. **153**, G587 (2006).
44. K. T. Tamai, H. Morinaga, T. K. Doi, S. Kurokawa, and O. Ohnishi, *J. Electrochem. Soc*. **158**, H333 (2006).

45. B. Park, H. Lee, K. Park, H. Kim and H. Jeong, *J. Materials Processing Technology*, **203**, 287-292 (2008).

46. D. Castillo-Mejia, J. Kelchner and S. Beaudoin, *J. Electrochem. Soc*. **151**, G271 (2004).

47. Y. C. Wang and T. S. Yang, *J. Electrochem. Soc*. **154**, H486 (2007).

48. D. Rosales-Yeomans, D. DeNardis, L. Borucki, T. Suzuki, Y. Sampurno, and A. Philipossian, *J. Electrochem. Soc*. **155**, H812 (2008).

49. G. P. Muldowney, *Mater. Res. Soc. Symp. Proc.* **Vol. 991**, 0991-C06-01 (2007).

50. G. P. Muldowney, *Mat. Res. Soc. Symp. Proc*. **Vol 991**, 0991-C06-01 (2007).

51. A. S. Lawing, *The Electrochem Soc. Proc*., **Vol. PV 2002-1**, 46 (2002).

52. A. S. Lawing, *Mat. Res. Soc. Symp. Proc*. **Vol 732**, I5.3 (2002).

53. A. S. Lawing, *CMP-MIC* (2002).

54. A. R. Baker, *Proceedings of the Second International Chemical Mechanical Planarization for VLSI/ULSI Interconnection Conference (CMP-MIC)*, San Jose, CA, 339-342 (1997).

55. D. Stain, D. Hetherington, M. Dugger and T. Stout, *J. Electronic Mater*. **25 (10)**, 1623-1627 (1996).

56. I. Ali and S. R. Roy, *Solid State Technology*, **40(6),** 185-191 (1997).